Materials Today Bio 31 (2025) 101492

Contents lists available at ScienceDirect

Materials Today Bio

journal homepage: www.journals.elsevier.com/materials-today-bio

Constructing a 3D co-culture *in vitro* synovial tissue model for rheumatoid arthritis research

Xiaocheng Wang [a,b,c,1], Jiaxin He [a,b,c,1], Qiang Zhang [a,b,c], Juan He [a,b,c], Qingwen Wang [a,b,c,*]

[a] Department of Rheumatism and Immunology, Peking University Shenzhen Hospital, Shenzhen, 518036, China
[b] Institute of Immunology and Inflammatory Diseases, Shenzhen Peking University-The Hong Kong University of Science and Technology Medical Center, Shenzhen, 518036, China
[c] Shenzhen Key Laboratory of Inflammatory and Immunology Diseases, Shenzhen, 518036, China

ARTICLE INFO

Keywords:
Rheumatoid arthritis
Synovial organoids
Drug screening
Fatty acid-binding protein 4
PI3K-AKT signaling pathway

ABSTRACT

The development and exploration of highly effective drugs for rheumatoid arthritis remains an urgent necessity. However, current disease research models are no longer sufficient to meet the rapid development of high-throughput drug screening. In this study, bacterial cellulose simulating the structure of extracellular matrix was used as a 3D culture platform, and THP-1-derived M1 macrophages, representing the inflammatory component, human umbilical vein endothelial cells (HUVECs), simulating the vascular component, and rheumatoid arthritis fibroblast-like synoviocytes (RA-FLSs), embodying the synovial pathology, were co-cultured to simulate the pathological microenvironment in RA synovial tissues, and synovial organoids were constructed. Under three-dimensional (3D) culture conditions, there was a notable upregulation of fatty acid-binding protein 4 (FABP4) in polarized macrophages, and an enhancement of pathological phenotypes in HUVECs and RA-FLSs, mediated through the PI3K/AKT signaling pathway, including cell proliferation, migration, invasion and vascularization. Compared to planar cultures and 2D co-cultures, 3D synovial organoids not only exhibit a broader range of transcriptomic features characteristic of rheumatoid arthritis but also demonstrate increased drug resistance, likely due to the more complex and physiologically relevant cell-cell and cell-matrix interactions present in 3D environments. This model offers a promising path for personalized treatment, accelerating precision medicine in rheumatology.

1. Introduction

Rheumatoid arthritis (RA) is an autoimmune disease with unknown pathogenesis, with multiple symmetric erosive arthritis as the main clinical manifestation, with a variety of autoantibodies in the body, obvious synovial hyperplasia and inflammatory cell infiltration, resulting in joint destruction and even extra-articular system damage [1,2]. Epidemiological surveys show that between 0.5 % and 1 % of patients with RA worldwide, and this number is increasing year by year, highlighting the growing public health challenge [3]. Due to its complex pathological mechanism, the research and development of therapeutic drugs for RA has always been an important challenge in the medical field [4]. Although large-scale sequencing technologies, such as genome, transcriptome, and proteome sequencing, have advanced research on RA , there are still shortcomings in adequately analyzing the complex and variable pathogenesis of RA and guiding individualized treatment [5]. Therefore, there is an urgent need to construct a low-cost and reproducible model that can realistically simulate the pathological microenvironment of synovial tissue in RA patients.

At present, the development of RA therapeutics mainly relies on cell models and animal models [6,7]. These research models can partially reflect the pathology *in vivo*, current 3D co-culture systems predominantly utilize non-human or immortalized cell lines, limiting their predictive accuracy for human arthritis processes and high-throughput drug screening capabilities. Moreover, cell models cultured in 2D planes lack the cell-matrix interactions present *in vivo*, leading to changes in morphology and gene expression loss during culture [8]. Previous attempts at constructing 3D synovial organoids primarily relied on

* Corresponding author. Department of Rheumatism and Immunology, Peking University Shenzhen Hospital, Shenzhen, 518036, China.
E-mail address: wangqingwen@pkuszh.com (Q. Wang).
[1] These authors contributed equally to this work.

https://doi.org/10.1016/j.mtbio.2025.101492
Received 12 May 2024; Received in revised form 25 November 2024; Accepted 12 January 2025
Available online 24 January 2025

Matrigel, which provides insufficient mechanical support, leading to a failure in maintaining structural integrity. This inadequacy worsens problems such as uneven cell distribution and poor cell encapsulation. Moreover, given that Matrigel originates from mouse tumor-derived extracellular matrix proteins, its application in drug development and regenerative medicine is constrained by tumor association, batch variability, cost, and safety concerns [9,10]. *In vivo* animal models need to consider not only the ethical and experimental costs, but also the complexity and accuracy of animal modeling. In addition, some countries, such as the United States, have made it clear that they will no longer fund projects based on animal models after 2035 [11].

Natural biomaterials for organoid construction offer replication of the *in vivo* microenvironment, enhanced cell-to-cell communication, structural support, and exposure to natural cues [12,13]. The unique properties of bacterial cellulose (BC) have drawn a lot of attention among the various biomaterials with varying characteristics and functions. These properties include high purity, high tensile strength, biocompatibility, formation of a 3D nanofibril network, excellent fluid exchange capabilities, cell adhesion and proliferation, lack of allergic reactions after implantation, and lack of evidence of toxicity or toxicity of degradation products. Furthermore, the fibrous and spongy structure of BC mimics the native tissue's extracellular matrix (ECM), featuring nanofibers comparable in size to ECM's collagen fibers but with reduced immunogenicity [14–16]. In addition, it can also be modified by exogenous compounds to present new properties. For example, plasma hydrophilic-modified polyester fiber can be used as the surface coating of BC to produce artificial blood vessels [17]. BC endowed with light-activated antimicrobial properties is produced via engineered microbial processes, serving as a living material designed for the repair of skin wounds [18]. In addition, after inoculation of adipose tissue on BC, the maturation of preadipocytes can be promoted, thus showing potential for adipose reconstruction [19]. Leveraging these properties, we propose using BC for constructing synovial organoids, a novel approach not previously explored.

In RA progression, FLSs are activated by inflammatory factors, chemokines, etc., such as TNF-α and IL-1β, secreted from immune cells including macrophages, dendritic cells, and T cells. Fatty acid-binding protein 4 (FABP4) is notably upregulated in synovial M1 macrophages in RA patients [20]. Elevated levels of FABP4 have been shown to promote pro-inflammatory signaling and cytokine secretion [21,22]. Furthermore, FABP4 levels in the serum and synovial fluid of RA and osteoarthritis (OA) patients are significantly higher and positively correlated with total cholesterol levels [23]. This activation promotes an inflammatory response and synovial invasion, suggesting that cellular communication between immune cells and FLSs plays an important role in RA pathogenesis [24,25]. Subsequently, FLSs autosecrete proinflammatory cytokines (e.g., IL-1α, IL-1β, IL-6), chemokines (e.g., CCL2, CXCL12), and tissue-damaging enzymes (including metalloproteinases and cathepsins). This autocrine and paracrine signaling facilitates the recruitment and activation of immune cells, such as macrophages, and vascular endothelial cells, further amplifying the inflammatory milieu and contributing to the degradation of joint tissues [26,27]. Inflamed synoviocytes and vascular endothelial cells penetrate the cartilage, initiating and intensifying the inflammatory reaction, leading to synovial inflammation [28].

Considering the crucial roles of macrophages, vascular endothelial cells, and synovial fibroblasts in the pathogenesis of RA, this study employs a co-culture of THP-1-derived M1 macrophages, HUVECs, and RA-FLSs to construct 3D synovial organoids in a natural BC matrix. This model aims to more accurately replicate the complex microenvironment of RA-affected synovium, overcoming limitations of traditional 2D cultures by demonstrating enhanced expression of FABP4 in M1 macrophages, which suggests a more pathologically relevant phenotype through the PI3K/AKT signaling pathway. The construction of synovial organoids not only provides a research platform for the screening of RA therapeutic drugs, but also provides new ideas and strategies for personalized treatment of RA, which has extensive practical needs and great social significance.

2. Experimental section

2.1. Preparation of BC

BC production involved utilizing Bacillus xylinus (ATCC 23 767). The culture medium was prepared by dissolving 5 g of glucose, 1 g of $MgSO_4 \cdot 7H_2O$, 5 g of mannitol, 5 g of polypeptone, and 5 g of yeast extract in 1 L of deionized water, with the pH adjusted to between 6.6 and 7.0. This medium was then autoclaved for 20 minutes. Subsequently, 5 mL of ethanol was added to the sterilized medium before it solidified. Bacillus xylinus was inoculated into the prepared culture medium and placed on a shaker table at 30 °C with a speed of 170 rpm for a duration of 7 days. After this period, activated liquid spawn was inoculated into fresh medium and incubated statically at 30 °C for 3–4 weeks to facilitate the production of BC. The harvested BC was then washed with deionized water to remove any residual medium. This was followed by boiling in a 1 % sodium hydroxide solution for 30 minutes and a final rinse in deionized water until a neutral pH was achieved.

2.2. Characterization of BC

The BC was prepared according to the methods reported before and its properties were characterized, including micro-morphology, stress-strain, elastic modulus, water contact angle, hydration degree, swelling ratio, etc [19,29]. Specifically, the hydrophilicity of BC was tested at room temperature using the sessile droplet method and observed using a goniometer and imaging system (SL200KB, Kino). After gold plating for 60 seconds, the structure and pore size of BC were characterized using a field emission scanning electron microscope (FE-SEM; Hitachi S-4800). Fourier transform infrared spectroscopy (FTIR, Nicolet Nexus 670, USA) was used to evaluate the surface chemistry of the BC in the wavenumber range of 4000-500 cm^{-1} at a resolution of 2 cm^{-1}. The spectra were further processed and mapped using Opus and Origin Pro 9.1 software. The mechanical properties of BC were characterized using a Hengyi tensile testing machine (HY-0230, China) equipped with a 100 N load cell.

2.3. Cell culture

Synovial tissue was collected from four patients with RA undergoing joint replacement surgery, and human primary RA-FLSs were prepared. The process was performed with the approval of the Human Research Ethics Committee of Peking University Shenzhen Hospital with approval number 2022-173. The other cell lines were derived from the National Collection of Authenticated Cell Culture (Shanghai, China). RA-FLSs and HUVECs were cultured with Dulbecco's Modified Eagle Medium (DMEM, Gibco, USA), and THP-1 was cultured in RPMI-1640 medium (Gibco, USA), all supplemented with 10 % fetal bovine serum (FBS, Gibco, USA).

2.4. Induction of THP-1 derived M1 macrophages

THP-1 cells were grown to a sufficient density, harvested by centrifugation, and then resuspended in complete medium comprising RPMI-1640 containing 100 ng/mL Phorbol-12-myristate-13-acetate (PMA, Solarbio, China). The cells were seeded in culture dishes for 24 hours to induce differentiation into Mφ-type macrophages. Subsequently, an induction medium containing 100 ng/mL Lipopolysaccharide (LPS, Solarbio, China) and PMA was prepared in RPMI-1640 and applied for 17 hours to promote further differentiation. The morphology of the cells was monitored under a microscope at each stage of induction.

2.5. Collection of M1 macrophage conditioned medium (CM)

THP-1 cells were seeded onto Petri dishes (2D) and BC (3D) and the cell amount was kept consistent, followed by induction of THP-1 into M1 macrophages. Discard the medium and wash off residual FBS and dead cells with PBS. Serum-free medium was then added, and supernatants from M1 macrophages were collected as CM after 16–18 hours, labeled as 2D-CM and 3D-CM, respectively. After a series of centrifugations to remove dead cells and debris, transfer the CM to a new EP tube and store in a −80 °C freezer.

2.6. Construction of synovial organoids

RA-FLSs, THP-1-derived M1 macrophages and HUVECs were seeded into Petri dishes and BC in a ratio of 3:1:1 and a density of 5×10^4 cells/cm^2 in BC. The number of cells in the single RA-FLSs control group was consistent with that of the other groups, and the culture was performed under normal conditions and the fresh medium was changed every 3 days until cell clumps appeared.

2.7. Histology and immunostaining

3D synovial organoids were fixed with 4 % paraformaldehyde, dehydrated using conventional methods, embedded in paraffin, and sectioned at a thickness of 7 μm to optimize histological detail and antibody penetration for subsequent staining. Sections were stained with hematoxylin and eosin (H&E). For immunofluorescence staining, 3D synovial organoids were embedded in OCT (4583, Sakura, Japan) for cryosectioning at 7 μm thickness. Sections were fixed in cold methanol and blocked with normal goat serum (G1208, Servicebio, China). The samples were then incubated overnight at 4 °C with primary antibody. The panel of antibodies included CD31 and CD86 (M1511–8 and T1606-50, Huabio, China), Vimentin and E-cadherin (10366-1-AP and 20874-1-AP, Proteintech, USA) and FABP4 (A0232, Abclonal, China). After washing the primary antibody, the fluorescently conjugated secondary antibody (FITC-AffiniPure Goat anti-rabbit bit IgG (H + L), Abcam, USA) was incubated at room temperature. Nuclei were counterstained with DAPI (28718-90-3, Solarbio, China) and then imaged under a confocal microscope (Leica, Germany). The nucleus was counterstained with DAPI (28718-90-3, Solarbio, China) and then imaged under confocal microscopy (Leica, Germany).

2.8. Tube formation assay

Matrigel (354230, BD Biosciences, Australia) was carefully added into the 24-well plate and incubated at 37 °C and 5 % CO_2 for 1h to cure the matrix glue. 7×10^4 HUVECs were mixed with macrophage CM and added into the well plate to observe the tube formation. When tube formation peaked, carefully remove the medium from the 24-well plate, being cautious not to damage the glue or cell network in the process. 100 μL of calcein am was added, diluted in serum-free media (1:500), incubated for 30 min away from light, washed with PBS and observe under a microscope. The parameters of tube formation were analyzed and quantified by AngioTool software.

2.9. Quantitative real-time PCR (RT-qPCR) assay

Cells were seeded into 6-well plates and treated with macrophage CM for 24 h and 48 h, respectively. Cells were collected, total RNA was extracted, and reverse transcribed into cDNA following the instructions of the manufacturer of the reverse transcription kit (AG11732, Accurate Biology, China). Endogenous β-actin was used as the reference gene and RT-PCR was performed on LightCycler 480 II. (Roche), and the relative expression levels of each gene were determined by $2^{-\Delta\Delta Ct}$ method. The primer sequences for RT-qPCR is shown in Table S1.

2.10. Immunoblotting

Cells were treated with CM and collected, lysed on ice using lysis buffer (Cowin Biotech Co., Ltd., China) containing phosphatase and protease inhibitors for 10 min. Proteins underwent separation through sodium dodecyl sulfate-polyacrylamide gel electrophoresis (SDS-PAGE), were transferred onto nitrocellulose membranes, and subsequently targeted with primary antibodies. Primary antibodies including anti-cyclin-dependent kinase 1 and 2 (CDK1 and CDK2; BF0091 and AF6237, Affinity, USA), anti-adipokine fatty acid-binding protein 4 and anti-vascular endothelial growth factors (FABP4 and VEGF, A0232 and A21647, Abclonal, USA), anti-cyclin-A2 and anti-cyclin-B1 (18202-AP and 28603-1-AP, Proteintech, USA), anti-vimentin (ab128507, Abcam, UK), anti-pi3k and anti-Phospho-pi3k (AF6242 and AF3242, Affinity, USA), anti-akt and anti-Phospho-akt (4691 and 4060, CST, USA) were used in this research. After incubation, the protein expression was detected by chemiluminescence method, and the image was collected by ChemiDocTM XRS+ (Bio-Rad, USA).

2.11. Drug resistance test

Drug resistance was assessed using four commonly prescribed rheumatoid arthritis medications: methotrexate (MTX), mycophenolate mofetil (MMF), leflunomide, and cyclosporine. The experiment was divided into three groups: (1) RA-FLSs were cultured alone in 2D dishes (control); (2) M1 macrophages, RA-FLSs, and HUVECs were co-cultured in 2D dishes (2D Co-culture); (3) M1 macrophages, RA-FLSs, and HUVECs were co-cultured on BC (3D Synovial organoids). The concentrations of the drugs were set at 2 μM (MTX), 12.5 μM (MMF), 25 μM (Leflunomide), and 2.5 μM (Ciclosporine). All medications are purchased from MedChemExpress (MCE, USA). Each experimental group was treated with drug for 48 hours and evaluated using live/dead assays and immunofluorescence staining.

2.12. RNA-sequencing (RNA-seq) analyses

After treating RA-FLSs and HUVECs with CM for 24 and 72 hours, cells were collected, and total RNA was extracted using Trizol. RNA quality control, library preparation, data evaluation, and assembly were performed by Novogene Co., Ltd. (Guangzhou, China). Differentially expressed genes (DEGs) were identified using the DESeq2 package. The selection criteria for DEGs were based on fold change (log2 fold change) and P value, with a threshold of $P < 0.05$ and FC > 2 or FC < 0.5 to identify significant genes. DEGs were visualized using heatmaps and volcano plots. Heatmaps were generated using the gplots R package, and volcano plots were created with the ggplot2 R package. GO enrichment analysis was conducted using clusterProfiler, while KEGG enrichment analysis was performed with Metascape, both with a significance threshold of $P < 0.05$.

2.13. Multiplex cytokine assays

The Bio-Plex Pro Human Cytokine Screening 48-plex Panel kit (12007283, Bio-Rad, USA) was utilized to detect cytokines in the supernatants of synovial organoid cultures using the Luminex 200 system (Luminex Corporation, USA). All experiments were repeated at least three times to ensure reproducibility.

2.14. Statistical analyses

Statistical analyses were performed on data collected from three independent experiments. Data are presented as mean ± standard deviation (SD). One-way analysis of variance (ANOVA) was performed using GraphPad software to assess the statistical significance of the results, a Tukey's HSD test was used for postoperative comparison, and the differences between the groups were further compared. The difference

was statistically significant: $*p < 0.05$, $**p < 0.01$ were statistically significant.

3. Results

3.1. Characterization of bacterial cellulose

BC produced by the fermentation of *Bacillus xylinus* (ATCC 23767), exhibits a fine nanonetwork structure with randomly intersecting nanofiber filaments, characteristic of BC hydrogels' 3D architecture and forming the physical basis of our *in vitro* culture platform (Fig. 1A–C; Figure. S1A, B). When BC is immersed in the medium, the color changes rapidly from transparent to light red, which is due to the three-dimensional network structure of BC that allows it to efficiently absorb and fix the surrounding liquid (Fig. 1E).

BC has good hydrophilicity and can promote cell adhesion (Figure. S1C), so the formation of clear cell prosthetic feet can be observed after culturing synovial organoids in BC, which is closely related to cell adhesion and motility (Fig. 1D–F, G). *In vivo* experiments have also proved that BC is very biocompatible and has broad application prospects (Figure. S1D). Fourier Transform Infrared Spectroscopy (FTIR) analysis of BC's molecular structure revealed absorption peaks between 3200 and 3500 cm^{-1} in the BC spectrum, primarily attributed to the tensile vibration of the hydroxyl group (O-H) caused by strong intramolecular and intermolecular hydrogen bonds. In addition, distinct adsorption peaks at 1632 and 1059 cm^{-1} correspond to acetyl groups and C=O stretching vibrations, respectively, underscoring the complex molecular interactions within BC that contribute to its biocompatibility (Fig. 1H) [30].

Nanofibers with a diameter of about 50–100 nm make up the porous structure of BC (average range of 60 %–80 %), so BC is ideal for providing nutrients and oxygen, which are necessary for cell development and phenotypic maintenance (Fig. 1L–N). Furthermore, despite its high porosity, BC possesses robust mechanical properties, withstanding strains from 20 % to 80 % (Fig. 1I and J). These exceptional mechanical capabilities provide a durable framework for synovial organoids, ensuring structural integrity and facilitating nutrient and oxygen transport to sustain cell growth and phenotype. The remarkable water absorption capacity and wettability of BC not only highlight its high water compatibility but also underline its potential as an ideal biological scaffold (Fig. 1K–M). These properties are crucial for maintaining a hydrated microenvironment conducive to cell survival and function, reinforcing BC's applicability in the construction and application of synovial organoids and beyond.

3.2. BC-based 3D culture facilitates cell communication

THP-1 monocytes have been widely used in the study of macrophages, during differentiation, THP-1 cells transitioned from a suspended to an adherent state, with a noticeable increase in cell elongation and clumping (Figure. S2A). CD86 was utilized for the identification of differentiated M1 macrophages through immunostaining (Figure. S2B). Flow cytometry analysis of CD80 further confirms the successful polarization of THP-1 cells into M1 macrophages (Figure. S2C, D). Additionally, the up-regulation of mRNA expression levels for key M1 macrophages markers, including CD86, CCL2, CCR7, IL-1β and TNF-α, was confirmed, underscoring the effective polarization towards a pro-inflammatory phenotype (Figure. S2E). At the same time, RT-qPCR experiments were also used to demonstrate the up-regulation of inflammation and angiogenesis related genes after macrophage polarization, which provided a theoretical basis for the selection of M1 macrophages to simulate the inflammatory environment (Figure. S2F, G). Immunofluorescence analysis revealed that primary cells isolated from RA synovial tissue exhibited high expression of vimentin, CD90, and FAP (Figure. S2H-J). In addition, Western blot results confirmed the elevated expression of CD55 and CD90, further indicating that the isolated primary cells are RA-FLSs (Figure. S2K, L).

To verify that BC-based 3D culture facilitates cell-to-cell communication, we collected conditioned medium from M1 macrophages cultured under different conditions to stimulate RA-FLSs and HUVECs, and observed the resulting changes in their phenotypes. Stimulation of RA-FLSs by M1 macrophage CM under different culture conditions (2D-CM and 3D-CM) promoted the changes of pathology-related phenotypes of RA-FLSs, including cell hyperproliferation, secretion of inflammatory and angiogenic factors, and enhanced migration and invasion. RT-qPCR experiments revealed significant upregulation of genes associated with inflammation (IL-1α, IL-1β, IL-6, and IL-8), angiogenesis (ANGPT1 and bFGF), cell cycle (CDK1 and CDK2), and migration and invasion (MMP9 and vimentin) following treatment with 2D-CM and 3D-CM (Fig. 2A and B). The abnormal proliferation of FLSs in RA is the main cause of synovial hyperplasia. Treatment with M1 macrophage CM under various culture conditions significantly promoted DNA replication in RA-FLSs, as evidenced by EdU assays (Fig. 2C), and the further supported by live-dead staining and CCK-8 assays, demonstrating enhanced cell proliferation (Figure. S3A-D). The transwell assay with or without Matrigel showed enhanced migration and invasion in the 2D-CM and 3D-CM groups compared to the control group (Fig. 2D–F). Wound healing assays showed that treatment of M1 macrophage CM promoted the migration of RA-FLSs (Figure. S4A-D), paralleling the aggressive behavior observed in synovial tissues of RA. We further measured the expression levels of cell cycle and migration-related proteins in RA-FLSs after M1 macrophages CM stimulation using western blotting, yielding results similar to those of RT-qPCR and transwell experiments (Fig. 2G and H).

Similarly, to verify that M1 macrophages were facilitated by cellular communication with HUVECs in 3D culture, HUVECs were stimulated with 2D-CM and 3D-CM, respectively. Our findings revealed significant upregulation of inflammation and angiogenesis-related genes expressions, indicating enhanced pathological responses in HUVECs. Notably, genes related to inflammation (IL-1α, IL-1β, and IL-6) and angiogenesis (ANGPT1 and ANGPT2), as well as cell cycle-related genes (cyclinB1 and CDK2), demonstrated significant upregulation. Interestingly, this upregulation intensified over time, from 24h to 72h of CM treatment, demonstrating a time-dependent pattern in gene expression (Fig. 3A; Figure. S5A, B). Angiogenesis in synovial tissue is a critical pathological event in the progression of RA. Through angiogenesis assays, we observed that CM stimulation significantly promoted vascular formation in HUVECs, as evidenced by increased branch point and netting number, highlighting the critical role of angiogenesis in RA pathology (Fig. 3B–D). Ki67 immunofluorescence staining, live-dead staining and CCK-8 experiments further confirmed that CM stimulation enhanced HUVECs proliferation (Fig. 3E; Figure. S3E, F). Additionally, flow cytometry detected that M1 macrophage CM promoted the cell cycle after treatment of HUVECs for 24 h or 72 h, indicating that M1 macrophage CM promoted the proliferation of HUVECs by regulating DNA replication and cell cycle progression (Figure. S6A-D). The transwell assay showed that CM treatment promoted the migration and invasion of HUVECs (Figure. S5C-E), which was consistent with the results of the scratch experiment (Figure. S7A, B). Western blot analysis further supported our findings, showing that 3D-cultured M1 macrophages significantly augmented the expression of proteins associated with inflammation, cell proliferation, angiogenesis, and the migratory and invasive capabilities of HUVECs (Fig. 3F and G).

3.3. BC-based 3D culture promotes cells with more RA-associated transcriptome signatures

To elucidate the *in vivo*-like pathological characteristics of RA-FLSs in a 3D inflammatory environment, we used CM from M1 macrophages cultured in 2D and 3D conditions to stimulate RA-FLSs and performed RNA sequencing. The volcano plot shows the expression level, length, type, and chromosome location of DEGs (differentially expressed genes)

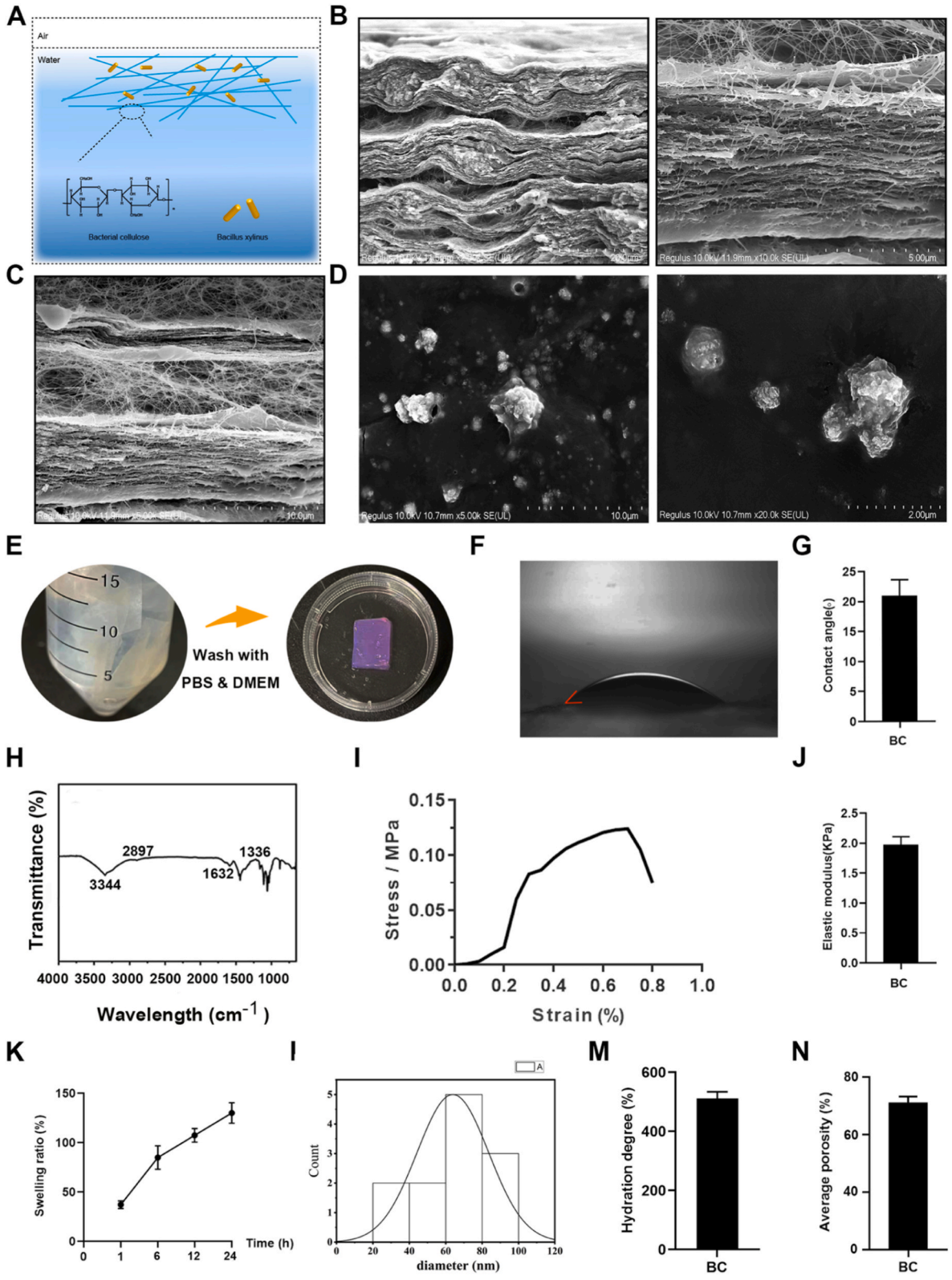

Fig. 1. Characterization of bacterial cellulose. (A) Schematic diagram of bacterial cellulose. (B, C) Side scanning electron microscopy (SEM) and microstructure of bacterial cellulose. (D) SEM image of synovial organoids on BC. The yellow framed portion represents structures similar to cell pseudopods. (E) Bacterial cellulose treatment flowchart. (F, G) The water contact angle and quantification of bacterial cellulose. (H) FTIR spectra of bacterial cellulose. (I) Stress–strain curves. (J) Elastic moduli. (K) Swelling ratio of bacterial cellulose at different time points. (L) Diameter distribution of nanofibers in bacterial cellulose. (M) Hydration degree of bacterial cellulose. (N) Average porosity of bacterial cellulose. (For interpretation of the references to color in this figure legend, the reader is referred to the Web version of this article.)

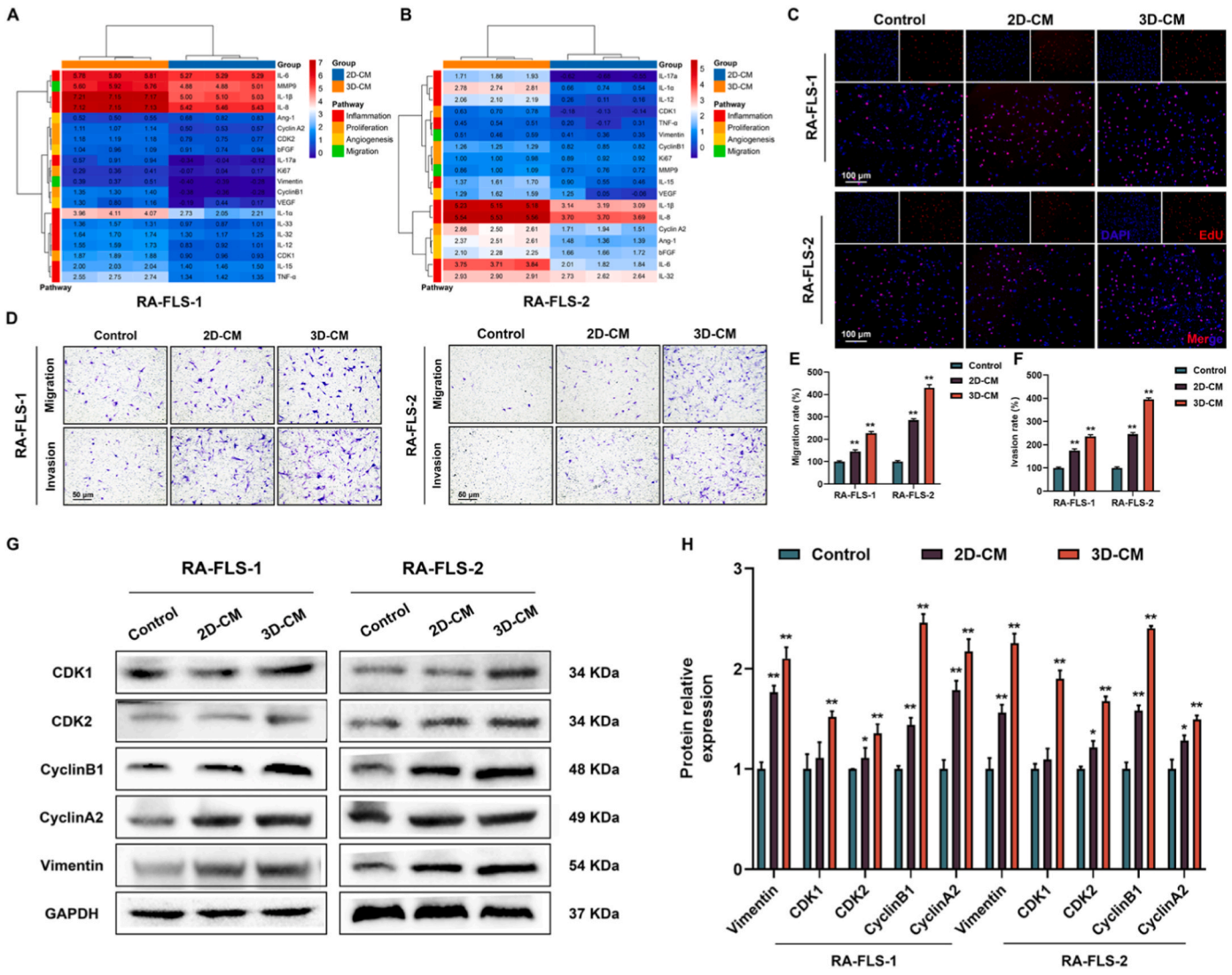

Fig. 2. 3D co-culture promotes the transition of RA-FLS-1 and RA-FLS-2 pathological phenotypes. (A, B) The relative expression of genes after 2D-CM and 3D-CM treatment of M1 macrophages for 24 h. The relative expression of the gene was further processed using Log2 transformation. (C) EdU detection of RA-FLSs after 24 h of 2D-CM and 3D-CM treatment. (D–F) Transwell assys showed that compared with the control group, the migration and invasion ability of RA-FLSs were increased after 48 h of 2D-CM and 3D-CM stimulation. (G, H) After treatment of RA-FLSs with 2D-CM and 3D-CM, the relative expression levels of cell cycle and migration-related proteins were analyzed by western blot. $*p < 0.05$ and $**p < 0.01$ compared to control. The data are shown as the mean ± SD.

between RA-FLSs treated with 2D-CM and 3D-CM and the control group (Fig. 4A). We found that in RA-FLS-1, after treatment with 2D-CM, 254 genes were upregulated and 148 genes were downregulated; after treatment with 3D-CM, 675 genes were upregulated and 516 genes were downregulated; comparing 2D-CM with 3D-CM, 351 genes were upregulated and 491 genes were downregulated (Figure. S8). In RA-FLS-2, after treatment with 2D-CM, 1584 genes were upregulated and 1779 genes were downregulated; after treatment with 3D-CM, 1802 genes were upregulated and 1774 genes were downregulated; comparing 2D-CM with 3D-CM, 854 genes were upregulated and 576 genes were downregulated (Fig. 4B).

Enrichment analyses conducted with the Kyoto Encyclopedia of Genes and Genomes (KEGG) identified significant enrichments in various signaling pathways, such as the PI3K/AKT signaling pathway, cytokine-cytokine receptor interaction, and apoptosis (Fig. 4C; Figure. S9C, D). Similarly, enrichment analyses utilizing the Gene Ontology (GO) revealed distinct gene enrichments across biological processes (BP), molecular functions (MF), and cellular components (CC). These included notable enrichments in the extracellular matrix and G-protein coupled receptor activity, among others (Fig. 4D; Figure. S9A, B). Further, GO enrichment analysis highlighted that DEGs predominantly associated with BP were significantly involved in cell chemotaxis and vascularization. In contrast, DEGs linked to CC and MF were primarily related to cytokine activity and extracellular matrix remodeling. This includes cytokine activity, chemokine activity, extracellular matrix, and proteinaceous extracellular matrix. KEGG enrichment analysis further revealed that the majority of the differentially enriched signaling pathways were related to the PI3K/AKT signaling pathway, cell cycle, RA, and DNA replication. Since 2D-CM and 3D-CM mimic the pathological microenvironment of RA mainly by promoting genes related to inflammation, angiogenesis, migration and invasion, and cycle, it is necessary to perform gene enrichment analysis on the upregulated genes separately. The results of enrichment analysis of up-regulated genes in RA-FLSs showed that GO and KEGG enrichment analyzed more RA-related signaling pathways (Figure. S10A-D).

To explore the transcriptomic characteristics of HUVECs in the inflammatory environment created by M1 macrophages under different culture conditions, we stimulated HUVECs with 2D-CM and 3D-CM and performed transcriptome sequencing. The volcano plot shows the expression level, length, type, and chromosome location of DEGs

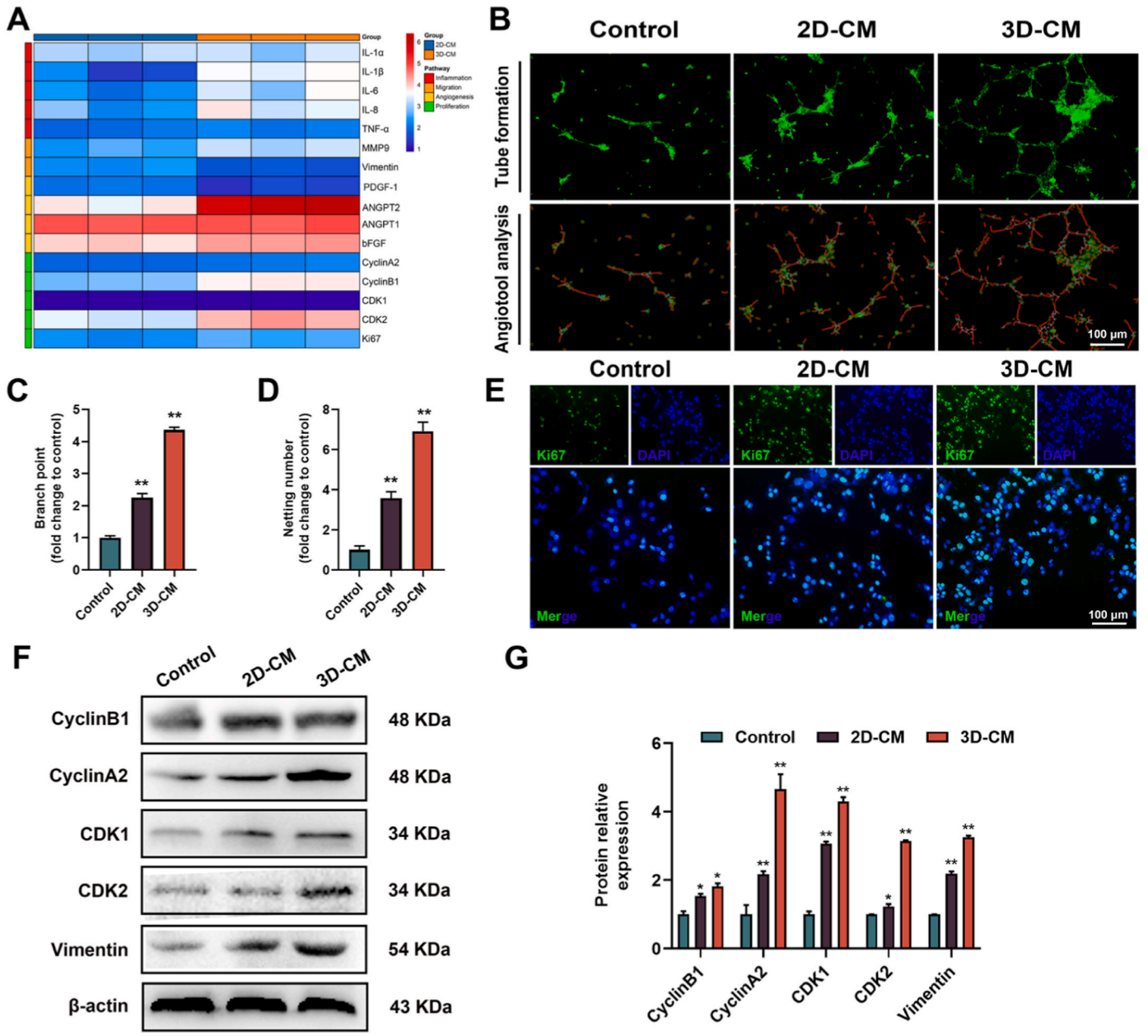

Fig. 3. 3D co-culture promotes the transition of HUVECs pathological phenotypes. (A) Relative gene expression of HUVECs after 72 h treatment of 2D-CM and 3D-CM. (B) Tube formation assay and AngioTool software quantification of HUVECs cultured with 2D-CM and 3D-CM. (C, D) Quantification of tube formation experiments, including branch point and netting number. (E) HUVECs were stained with Ki67 immunofluorescence after 24 h of 2D-CM and 3D-CM treatment. (F, G) After treatment of HUVECs with 2D-CM and 3D-CM, the relative expression levels of cell cycle and migration-related proteins were analyzed by Western blot. $*p < 0.05$ and $**p < 0.01$ compared to control. The data are shown as the mean ± SD.

between RA-FLSs treated with 2D-CM and 3D-CM and the control group (Fig. 5A). We found that 1397 genes were up-regulated and 1433 genes were down-regulated after 2D-CM treatment in HUVECs, 2502 genes were up-regulated and 3422 genes were down-regulated after 3D-CM treatment, and 11731 genes were up-regulated and 2103 genes were down-regulated when compared with 2D-CM and 3D-CM (Fig. 5B).

GO enrichment analysis showed that the main enrichment of DEGs related to biological processes was cell chemotaxis, vascularization and chemokine-mediated signaling pathway, while the DEGs related to Cellular Component and Molecular Function mainly involved in cytokine activity and extracellular matrix remodeling, including cytokine activity, chemokine activity, extracellular matrix, etc (Fig. 5C; Figure. S11A). KEGG enrichment studies showed that most of the differentially enriched signaling pathways were related to PI3K/AKT signaling pathway, cell cycle, RA, etc (Fig. 7D; Figure. S11B). Disease enrichment analysis of DO and DisGNET showed that it was mainly enriched in inflammation, tumor angiogenesis, arthritis, etc (Figure. S12A-D). The results of enrichment analysis of up-regulated genes in HUVECs showed that GO and KEGG enrichment analyzed more signaling pathways associated with RA (Figure. S13A-D).

3.4. *FABP4 promotes the transformation of cellular phenotypes*

Based on previous studies identifying FABP4 in M1 macrophages as a promoter of RA synovitis, angiogenesis, and cartilage degradation, thereby exacerbating disease progression *in vivo* and *in vitro*, we next explored whether alterations in the pathological phenotype of RA-FLSs and HUVECs were associated with increased FABP4 secretion in M1

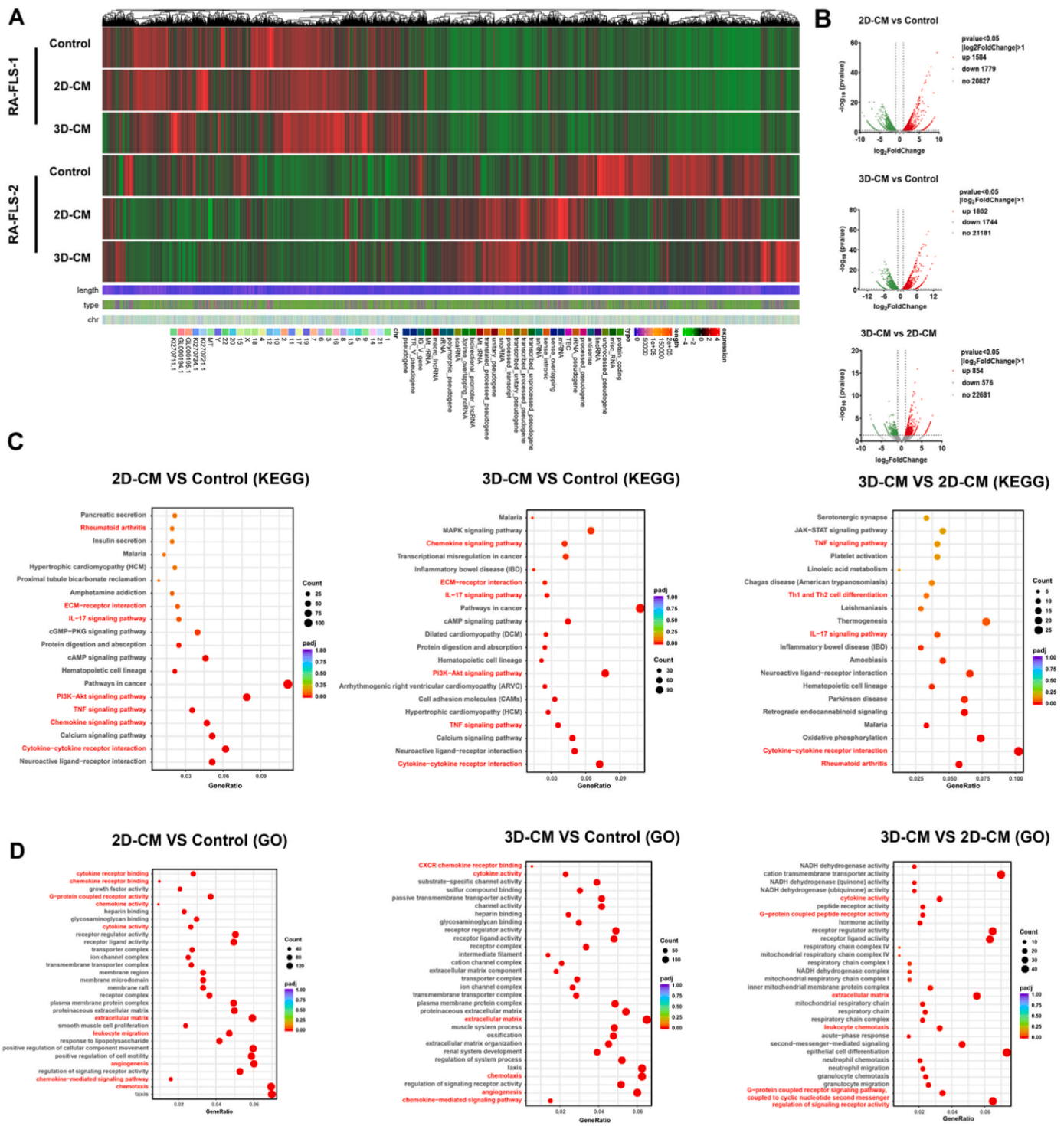

Fig. 4. Transcriptomic characterization of RA-FLSs in 3D synovial tissue. (A) The clustered heatmap shows the differentially expressed genes of RA-FLSs after 2D-CM and 3D-CM treatment. (B, C) The volcano plot represents the differentially expressed genes of RA-FLS-2 after 2D-CM and 3D-CM treatment compared with the control group. (D) Kyoto Encyclopedia of Genes and Genomes (KEGG) enrichment analyses showed enrichment in different signaling pathways, including IL-17 signaling pathway, TNF signaling pathway, PI3K/AKT signaling pathway, Chemokine signaling pathway, RA, etc. (E) Gene ontology (GO) enrichment analyses showed differential gene enrichment in biological processes, molecular functions, and cellular components, including chemokine activity, cytokine activity, chemotaxis, leukocyte migration, angiogenesis, etc.

macrophages [20]. Initially, we examined the expression of vimentin (a marker of RA-FLSs) and CD31 (a marker of vascular endothelial cells) in the synovial tissues of two RA patients using immunofluorescence to assess RA pathology. We observed elevated levels of vimentin and CD31 in human RA synovial tissue, indicating increased proliferation and invasion of RA-FLSs and enhanced angiogenesis within the synovial tissue. (Figure. S14A, B). Concurrently, we noted high FABP4 expression, with similar patterns of elevated FABP4 and vimentin expression observed in the joints of CIA mice (Figure. S14C, D), suggesting FABP4's involvement in the proliferation, migration, and invasion of synovial fibroblasts and vascular endothelial cells, as well as in inflammation and angiogenesis.

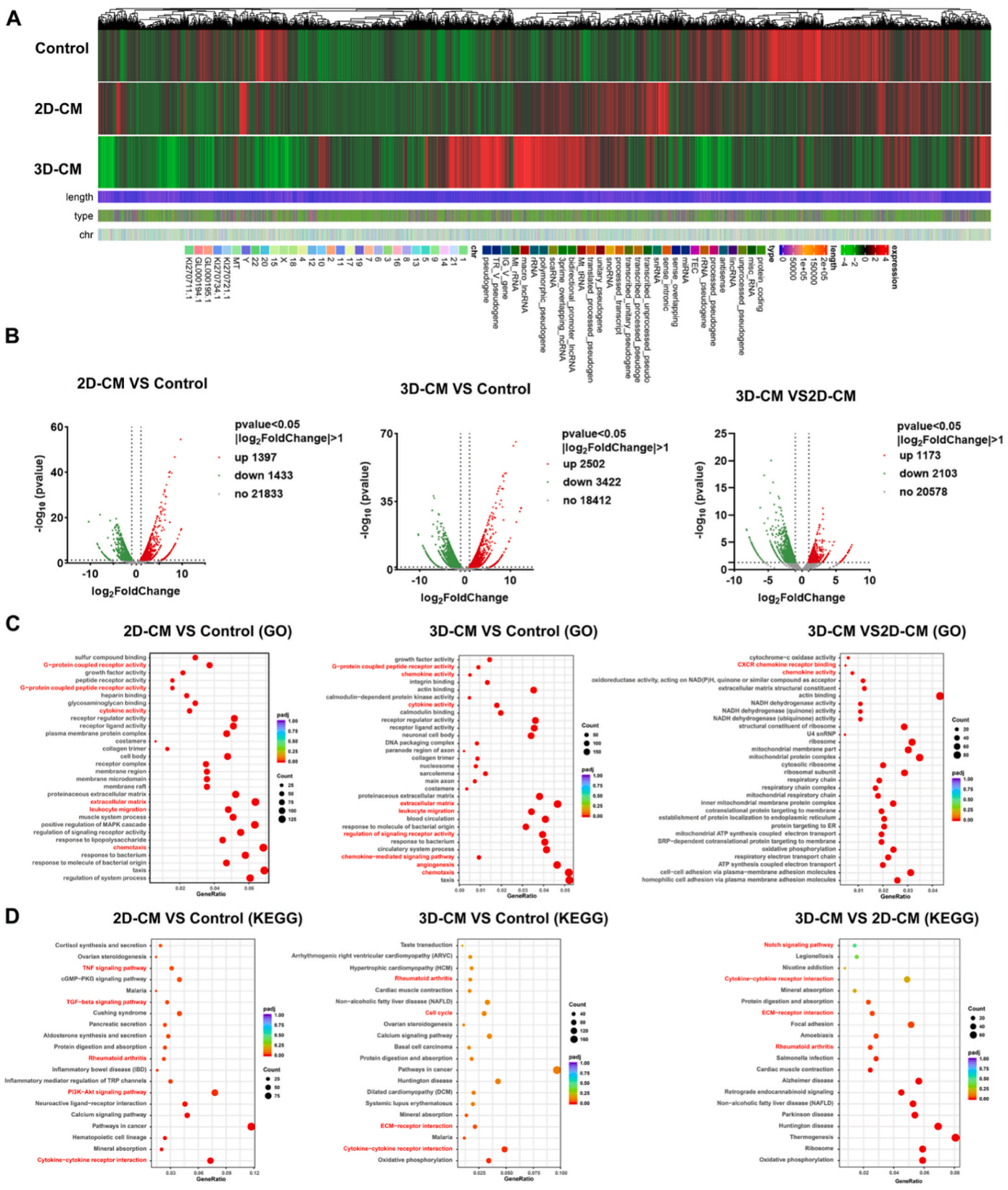

Fig. 5. Transcriptomic characterization of HUVECs in 3D synovial tissue. (A) The heat map shows the differentially expressed genes of HUVECs after 2D-CM and 3D-CM treatment. (B) The volcano plot represents the differential expression of genes in HUVECs after 2D-CM and 3D-CM treatment compared to the control group. (C) GO enrichment analyses showed differential gene enrichment in biological processes, molecular functions, and cellular components, including cytokine activity, chemotaxis, leukocyte migration, angiogenesis, etc. (D) KEGG enrichment analyses showed enrichment in different signaling pathways, PI3K/AKT signaling pathway, Notch signaling pathway, TGF-β signaling pathway, cell cycle, RA, etc.

To determine whether the pathological phenotype transformation of RA-FLSs and HUVECs induced by 3D-CM from M1 macrophages is linked to FABP4 upregulation, we analyzed FABP4 expression in M1 macrophages cultured in 2D and 3D environments using western blot and RT-qPCR. The results indicated that 3D culture conditions significantly enhanced FABP4 expression. (Figure. S14E-G). To further ascertain the link between cell phenotype changes and FABP4 overexpression, we introduced the FABP4 inhibitor BMS309403 into the M1 macrophage CM and evaluated its impact on RA-FLSs and HUVECs. Initial toxicity assessments of BMS309403 on HUVECs and RA-FLSs, using the CCK-8 assay at 20 μM doses, showed no toxicity after 24, 48, and 72 h (Figure. S15A-C).

Subsequent experiments revealed that the addition of BMS309403 to M1 macrophage CM inhibited the migration and invasion of RA-FLSs (Figure. S16A-C; Figure. S17A-D), along with downregulation of genes related to inflammation, angiogenesis, cell cycle, and cell migration and invasion (Figure. S16D-K). Additionally, western blot analysis indicated that cell cycle-related proteins, including cyclin B1, cyclin A2, CDK1,

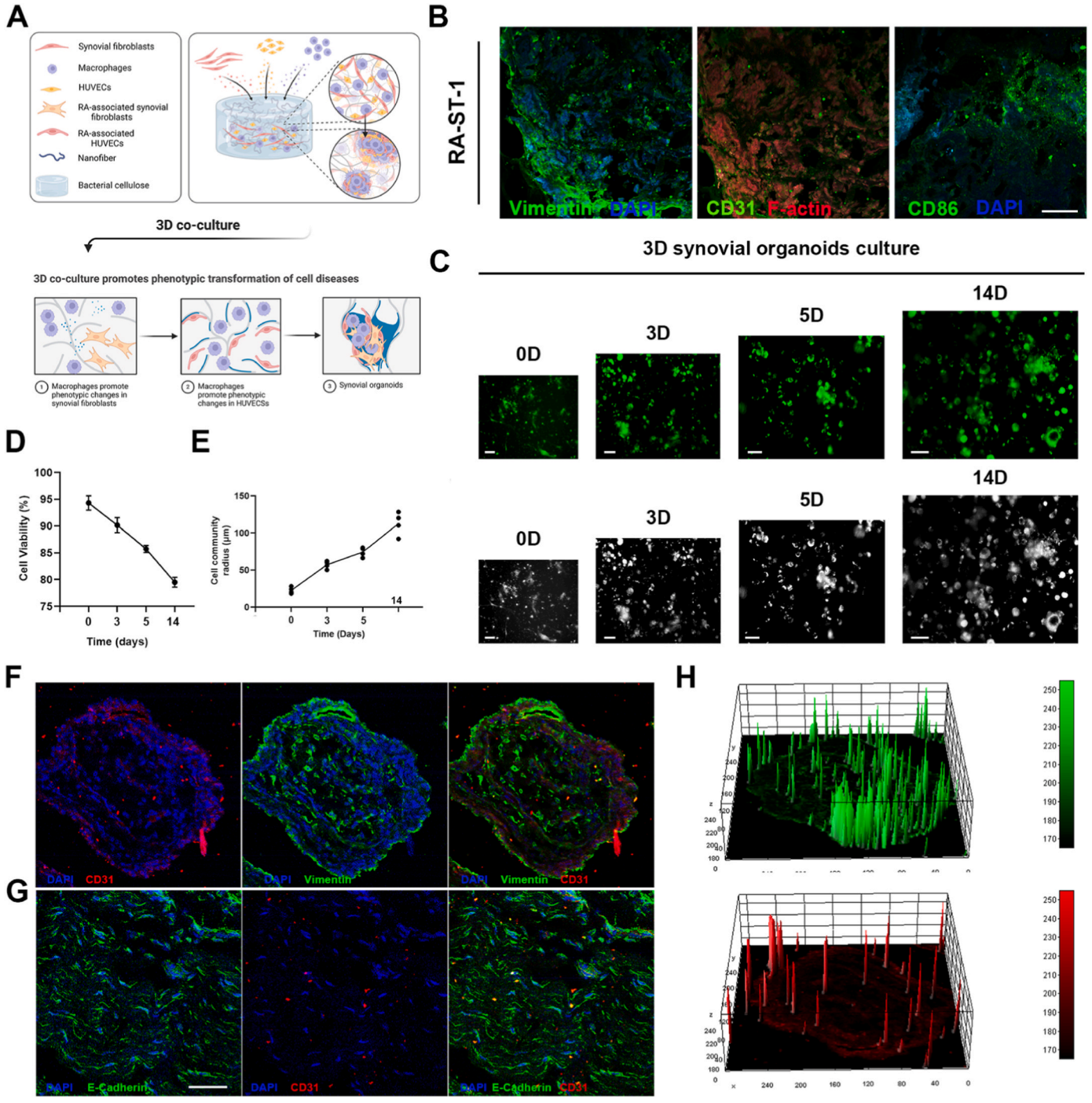

Fig. 6. Characterization of 3D synovial organoids. (A) Schematic diagram of synovial organoids constructed by co-culturing RA-FLSs, HUVECs and macrophages on BC. (B) Immunofluorescence staining was performed on vascular endothelial cell markers (CD31), synovial fibroblast markers (Vimentin) and M1 macrophage markers (CD86) in synovial tissues of RA patients. (C–E) Cell viability and morphology analysis of organoids during 14 days of continuous culture on BC. (F) Immunostaining of specific proteins in organoids, including vimentin and CD31. (G) Immunostaining of specific proteins in organoids, including CD31 and E-cadherin. (H) Image J analysis shows the spatial expression of vimentin and CD31 in synovial organoids.

and CDK2, were downregulated following BMS309403 treatment (Figure. S16L, M).

In HUVECs, angiogenesis was suppressed following BMS309403 addition, as shown by a decrease in vessel-like structure formation, total vessel length, and average vessel length (Figure. S18A-G). EdU results confirmed that BMS309403 also inhibited DNA replication in HUVECs (Figure. S18H, I). Moreover, transwell and scratch assays demonstrated reduced cell migration and invasion (Figure. S18J-L; Figure. S19A, B), while RT-qPCR analysis revealed downregulation of genes associated with inflammation, angiogenesis, the cell cycle, and cell migration and invasion (Figure. S18M, N, Q). Western blot findings further confirmed the downregulation of proteins related to angiogenesis, migration, invasion, and the cell cycle upon BMS309403 addition, reinforcing the inhibitor's efficacy in modulating pathological phenotypes related to RA (Figure. S18O, P).

3.5. FABP4 upregulates PI3K/AKT pathway in HUVECs and RA-FLSs

The progression of RA is linked to the abnormal activation of the PI3K/AKT signaling pathway, which plays a pivotal role in regulating cell proliferation, apoptosis, and differentiation [31]. Our transcriptome analysis revealed that the pathological phenotype transformation in HUVECs and RA-FLSs, induced by M1 macrophages, was primarily associated with the PI3K/AKT signaling pathway. Further analysis indicated that the addition of an FABP4 inhibitor reversed the cytopathological phenotype changes, suggesting a potential link between FABP4-regulated cytopathological changes and the PI3K/AKT signaling pathway. To substantiate this hypothesis, we conducted western blot analyses to examine the expression of proteins related to the PI3K/AKT signaling pathway with and without FABP4 inhibitors. The findings confirmed that CM from M1 macrophages upregulated the expression of PI3K/AKT signaling pathway-related proteins in both HUVECs and RA-FLSs. Conversely, the presence of FABP4 inhibitors led to the suppression of these proteins' expression (Figure. S20A-C), demonstrating that 3D culture conditions facilitate FABP4 secretion, which subsequently influences the PI3K/AKT signaling pathway, resulting in more pronounced pathological phenotypes in HUVECs and RA-FLSs.

3.6. Characterization of 3D synovial organoids

In the above studies, we have confirmed that compared with 2D culture, BC-based 3D culture promotes information exchange between cells, specifically, 3D culture promotes the secretion of FABP4, which further affects the changes of pathology-related phenotypes of RA-FLSs and HUVECs. Based on these studies, we optimized the culture conditions of organoids and demonstrated the superiority of co-culture, which can better simulate the pathological microenvironment *in vivo* (Fig. 6A).

To validate that these synovial organoids replicate the pathological environment of RA patient synovial tissues accurately, we conducted immunostaining on synovial tissues from two RA patients. Confocal laser scanning microscopy revealed high expression levels of vimentin, CD31, and CD86, highlighting the inflamed, proliferative, and highly vascularized nature of RA synovial tissue (Fig. 6B; Figure. S21A). In the 3D co-culture, cell aggregates formed spherical spheroids of uniform size with smooth, well-defined boundaries as culture duration increased, maintaining high cell viability throughout the organoid construction (Fig. 6C–E; Figure. S21B). Although small monocellular islands appeared within the organoid during its formation, the predominant structure was characterized by the co-presence of the three cell types, expressing high levels of vimentin, CD31, and E-cadherin, suggesting that the organoids closely mimic the pathological microenvironment of RA synovial tissue (Fig. 6F–H).

Next, we analyzed the culture supernatants of synovial organoids under various conditions, measuring the secretion of 48 factors, including inflammatory cytokines, chemokines, and angiogenesis factors, using Luminex 200 (Fig. 7A). The cytokine heatmap indicated that secretion levels of inflammatory and angiogenic factors, and chemokines by the 3D synovial organoids and the 2D co-culture group were significantly higher than those by the single RA-FLSs group, demonstrating enhanced cell-cell communication in co-culture conditions (Fig. 7B). Notably, the secretion of inflammatory factors (IL-1α, IL-1β, IL-6, IL-8), chemokines (MCP-3, MIG, M-CSF), and angiogenesis factors (HGF, VEGF) increased manifold compared to the control group (Fig. 7C–N; Figure. S21C-N). The elevated secretion of IL-6, a key pro-inflammatory molecule in RA, in synovial organoids, may further stimulate the secretion of other inflammatory factors and chemokines, sustaining a highly inflammatory pathological environment within the organoids.

3.7. Application of synovial organoids in drug screening

To assess the potential of synovial organoids as a drug screening platform, we tested four clinical drugs: MTX, MMF, leflunomide, and cyclosporine, for drug resistance. The impact of each drug on the viability of RA-FLSs cultured on a flat surface was determined using the CCK-8 assay to identify suitable drug concentrations (Fig. 8A–D). Live/dead staining revealed that cells within synovial organoids exhibited higher survival rates and lower mortality than those in single 2D and 3D cultured RA-FLSs (Fig. 8E). This increased drug resistance in 3D synovial organoids is likely due to their complex cellular architecture and extracellular matrix (ECM), which better mimic the *in vivo* synovial microenvironment and provide protective niches for cells. This highlights the advantage of 3D organoids as a more physiologically relevant platform for drug screening, enabling the evaluation of drug efficacy under conditions that closely resemble those in actual RA-affected tissues.

Overall, this study demonstrates the construction of synovial organoids using BC, where 3D culture enhances cell-cell interaction, effectively replicating the RA synovial tissue's pathological microenvironment. Thus, these organoids not only offer insights into the disease's onset and progression but also present a promising drug screening platform to advance RA research (Fig. 9A and B).

4. Discussion

RA is a widespread and chronic autoimmune disease marked by progressive and intermittent inflammation of the synovium, leading to the degradation of synovial joints with an unclear etiology [32]. The complex pathophysiology of RA presents a significant challenge to the development of effective therapeutics in the biomedical field.

Currently, RA research relies on cell and animal models. Traditional 2D cell models, while useful, often result in altered cell morphology and gene expression due to the lack of cell-matrix interactions [8]. The 3D model is mainly constructed by laying the matrix components and adding synovial fibroblasts, and the two-step method results in the matrix not being able to wrap the cells, and there is a situation where the cells are unevenly distributed. In addition, this single-cell model lacks disease-related stromal cells, including vascular endothelial cells and immune cells, which is not conducive to studying the interaction between cells and their stromal environment, and cannot faithfully mimic the pathological environment *in vivo* [33]. Animal models, despite their utility, are constrained by ethical considerations, financial implications, and the inherent challenges of mirroring disease complexity and fidelity [34]. Innovations in biomaterials and tissue engineering, including 3D printing, bioink technologies, and decellularized matrices, have been integrated into organoid culture methodologies, enhancing the field of organoid research [35]. These advanced 3D organoid models encapsulate the structural and functional essence of native tissues, incorporating vascular and tissue heterogeneity, thereby more effectively simulating cell-matrix and cell-cell interactions [36,37]. Furthermore, these models offer customizable features, allowing for the simulation of various disease stages through the manipulation of material properties and culture

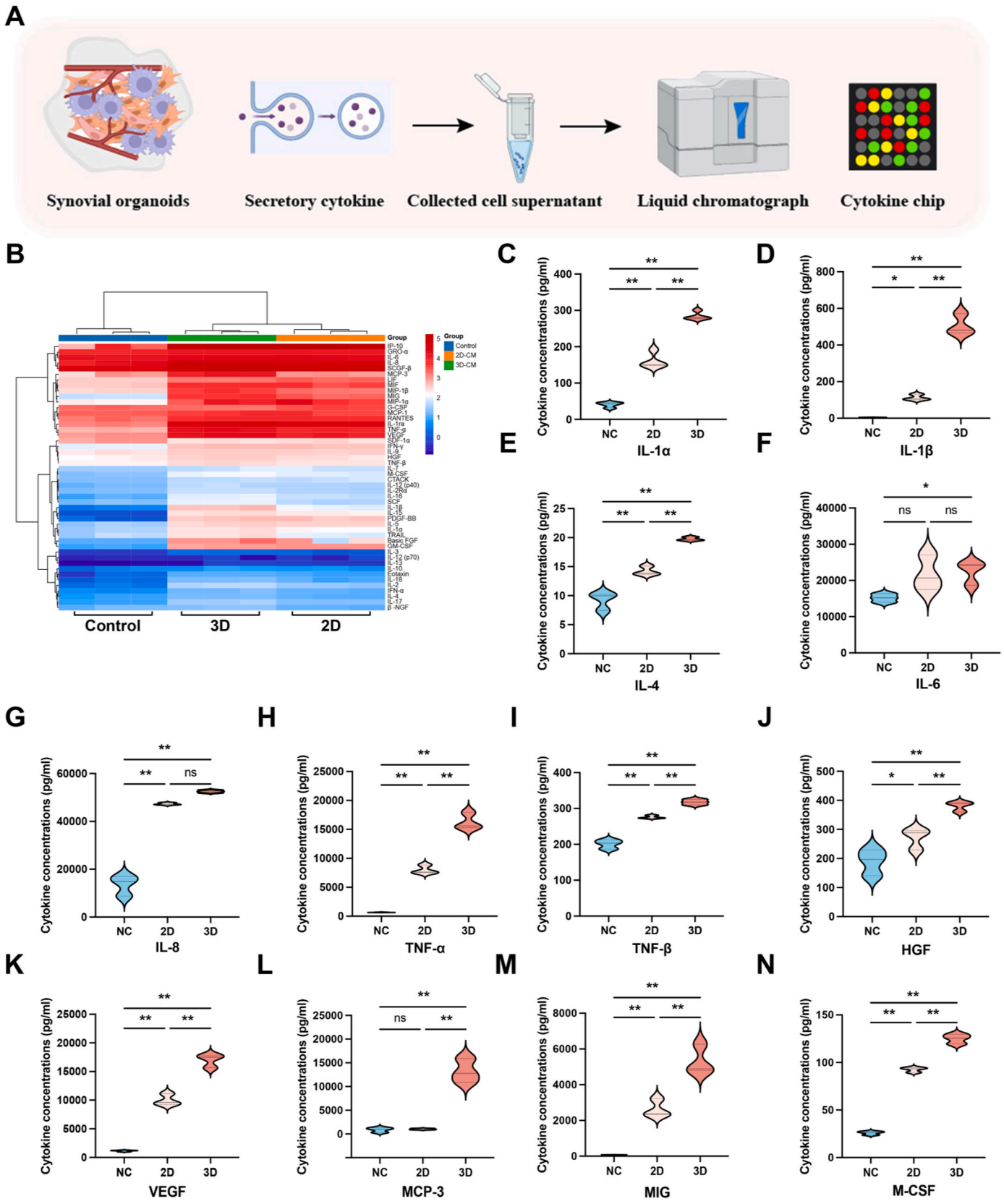

Fig. 7. Characterization of secretory function of synovial organoids. (A) Schematic diagram of the determination of synovial organoid secretion factors using a liquid microarray. (B) The heatmap shows the relative secretion of multiple cytokines between groups. (C–I) Secretion of inflammatory factors, including IL-1α, IL-1β, IL-4, IL-6, IL-8, TNF-α, TNF-β. (J, K) Secretion of angiogenic factors, including HGF and VEGF. (L–N) Secretion of chemokines, including MCP-3, MIG and M-CSF. $*p < 0.05$ and $**p < 0.01$ compared to control. The data are shown as the mean ± SD.

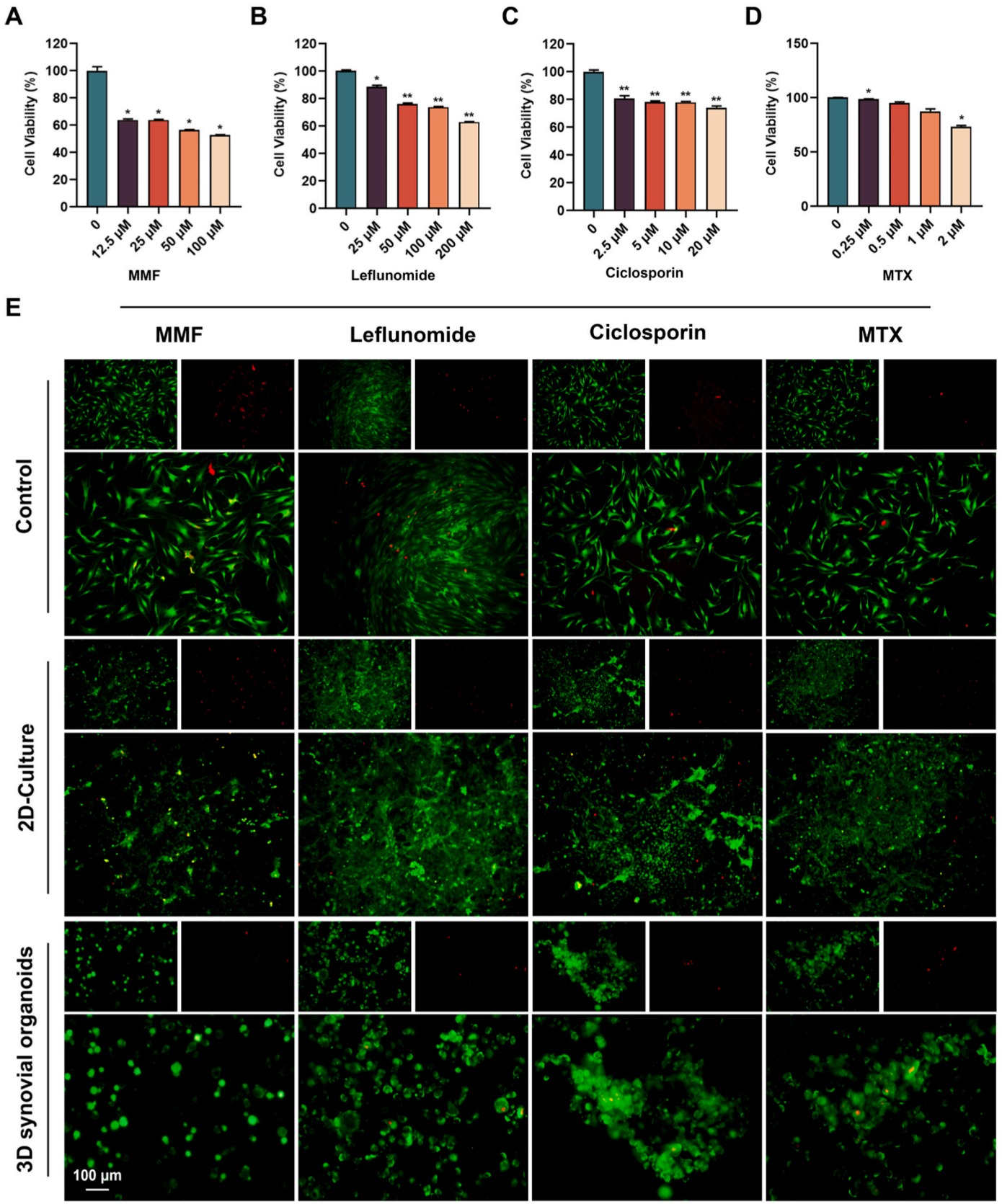

Fig. 8. Drug testing of 3D synovial organoids. (A–D) Cell viability after treatment of RA-FLSs with different rheumatoid clinical drugs, including mycophenolate mofetil (MMF), leflunomide, cyclosporine and methotrexate (MTX). (E) Live/dead staining of RA-FLSs grown in different culture conditions after rheumatoid clinical drugs treatment (green = live cells, red = dead cells). *$p < 0.05$ and **$p < 0.01$ compared to control. The data are shown as the mean ± SD. (For interpretation of the references to color in this figure legend, the reader is referred to the Web version of this article.)

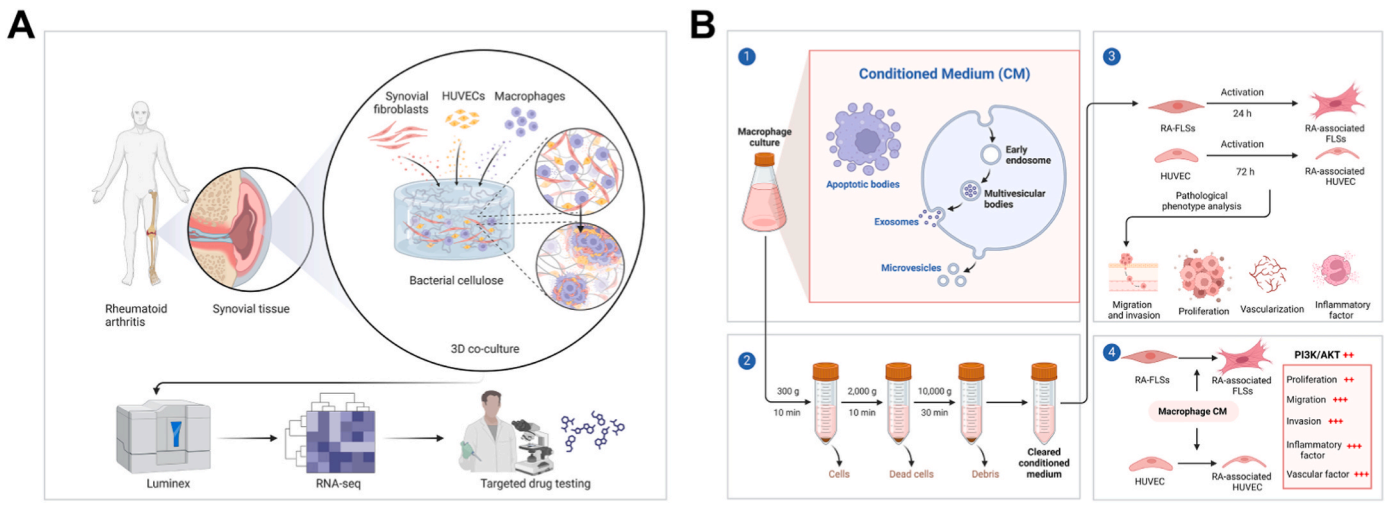

Fig. 9. To elucidate the working model of the construction and functional exploration and application of 3D synovial organoids. (A) Schematic diagram of the impact of cell co-culture on the phenotypic changes of cells. (B) Schematic diagram of the construction of 3D synovial organoids and the exploration of their function and application. This graphical abstract was delineated with the aid of the Biorender website (https://biorender.com/).

conditions [38]. Therefore, biomaterial-based 3D tissue models are a new direction in organoid research, facilitating large-scale drug testing and heralding a new era of personalized medicine. This shift demonstrates the potential of 3D organoid models to bridge the gap between traditional *in vitro* studies and clinical applicability, aiding in the study of the pathogenesis of RA and paving the way for the development of targeted therapeutic interventions.

The pathological microenvironment of synovial tissue plays a key role in the progression of RA and response to treatment. In the pathological state, the microenvironment transmits various stress signals, leading to an inflammatory response in synovial cells. Components such as FLSs, macrophages, and vascular endothelial cells (VEC) interact to release large amounts of stromal cell-derived factors, pro-inflammatory cytokines, and pro-angiogenic factors. This complex interaction exacerbates the proliferation and invasion of synovial cells, stimulates angiogenesis, accelerates bone erosion, and drives the pathological process in RA joints [39]. Therefore, Philippon et al. utilized collagen-based 3D scaffolds to culture RA fibroblast-like synovial cells (RA-FLSs), human umbilical vein endothelial cells (ECs), and monocyte-derived macrophages to construct synovial organoid models [40].

In this study, we have innovatively developed a bacterial cellulose-based cell co-culture organoid model utilizing patient-derived cells. This model facilitates the examination of cell-cell crosstalk within the arthritis context, marking a significant advancement in arthritis research. The co-culture system leverages the advantages of 3D organoid models, enabling the exploration of functional and spatiotemporal interactions among diverse cell populations [41,42]. BC serves as a multifunctional scaffold, enhancing cell interactions crucial for growth, migration, invasion, inflammatory cytokine production, pre-vascularization, and the reconstruction of the pathological microenvironment. Through 3D co-culture, we successfully replicate the *in vivo* synovial tissue microenvironment, accurately restoring critical signaling pathways such as PI3K/AKT. This flexible system, capable of simulating the synovial pathological environment, presents a novel platform for continuous monitoring of synovial development in RA and for conducting drug screenings.

Owing to its biocompatibility and resemblance to the extracellular matrix, BC is extensively utilized in tissue engineering and organoid construction, promoting cell growth and cytokine secretion through its soft matrix environment and multidimensional cellular contacts. Utilizing the THP-1 human monocyte line, renowned for its application in studying human diseases like osteoarthritis and other inflammatory conditions [43], we induced M1 macrophages to mimic the RA synovial tissue's inflammatory milieu. Our co-culture approach, which fosters interactions among multiple cell types within a shared milieu, revealed that 3D-cultured M1 macrophages significantly alter the pathological phenotypes of RA-FLSs and HUVECs [44]. These changes encompass increased secretion of inflammatory factors, enhanced cell proliferation, migration, invasion, and pre-vascularization, crucial for mirroring *in vivo* signal transduction [33]. Furthermore, gene enrichment analysis conducted on transcriptome sequencing data highlighted that the genes and signaling pathways influenced by 3D-cultured M1 macrophages, particularly those associated with RA, encompass DNA replication, cell cycle regulation, apoptosis, PI3K/AKT, Notch signaling, vascularization, chemokine and cytokine activity, and chemotaxis. Therefore, our organoid model shares a similar cell composition with that of Philippon et al., but without the addition of exogenous growth factors. Furthermore, we not only investigated the effects of different culture conditions on cellular behavior, but also revealed that 3D culture conditions upregulate FABP4 in macrophages, which modulates RA-related pathological phenotypes through the PI3K/AKT signaling pathway, providing a theoretical foundation for model construction and drug development. This comprehensive analysis underscores the model's potential in elucidating the molecular mechanisms underpinning RA's pathological phenotypic changes, offering valuable insights into disease progression and therapeutic targeting.

Our findings extend the understanding of FABP4, traditionally recognized as an adipogenic factor secreted by polarized macrophages [23,45]. Our study further demonstrated that FABP4 secretion was significantly enhanced in M1 macrophages under 3D culture conditions. This secretion likely benefits from the unique morphology of bacterial cellulose, marking a significant advancement in synovial organoid development. More importantly, FABP4 affects the pathological features of RA-FLSs and HUVECs through the PI3K/AKT signaling pathway, thereby exacerbating RA-related inflammatory responses. The PI3K/AKT signaling pathway plays a core role in the regulation of cell growth, survival, migration, and metabolism. In recent years, more and more studies have revealed the importance of the PI3K/AKT signaling pathway in the pathological process of RA, especially in the regulation of inflammation and immune response. Our study found that FABP4 affects the pathological characteristics of RA-FLSs and HUVECs through the PI3K/AKT signaling pathway, further revealing the core regulatory role of this signaling pathway in RA. Activation of the PI3K/AKT signaling pathway may be an important mechanism for the enhanced inflammatory response induced by FABP4 and the changes in RA-related cell

functions. With this finding, our study reveals the critical role of FABP4 in the rheumatoid arthritis microenvironment, further supporting the feasibility of FABP4 as a potential therapeutic target.

3D synovial organoids have demonstrated enhanced sensitivity and predictability in drug testing over 2D models. This aligns with findings that organoids' manageable size contributes to their heightened drug responsiveness [35]. Furthermore, our organoids offer a more homogeneous platform for drug screening, potentially overcoming the heterogeneity challenges observed in native tissue models [46]. The 3D synovial organoids offer numerous benefits compared to systems where different cell types are cultivated in similar dimensional environments, despite the demonstrated impact of 3D scaffolds on drug delivery [47].

While our study successfully models the interactions among endothelial cells, macrophages, and fibroblast-like synoviocytes (FLSs), which are critical components of the synovial microenvironment in rheumatoid arthritis (RA), we acknowledge its limitations. Key immune cell populations, such as T helper cells (Th1 and Th17), B cells, and osteoclasts, also play significant roles in RA pathogenesis, and their exclusion from this model limits the scope of our findings. Future studies should aim to incorporate these additional immune cell types into the organoid model to capture the broader complexity of cellular interactions that contribute to RA pathology. In addition, we used THP-1-derived M1 macrophages to simulate the inflammatory environment in RA synovial tissue, which is a commonly used and highly operable model. However, we also recognize that synovial macrophages (MLS) have more complex polarization states and diverse functions, and their origin and dynamics are significantly different from THP-1 macrophages. The latest studies have shown that MLS plays an important role in RA pathology [48]. In the future, we plan to introduce more physiologically relevant MLS cells into the model and combine high-throughput technology to further analyze the complex functions and cellular interactions of synovial macrophages. By doing so, we can achieve a more comprehensive understanding of RA mechanisms and identify novel therapeutic targets that involve these immune cell populations.

In summary, our 3D synovial organoid model replicates the synovial tissue's physiological and pathological states, offering a valuable tool for clinical treatment research. Its advantages in drug delivery and responsiveness underscore its potential as a superior model for RA therapy development.

5. Conclusion

In conclusion, this study successfully created a controllable *in vitro* 3D synovial organoid model that mimics the RA pathological environment through the innovative use of BC and co-culture of RA fibroblast-like synovial cells, M1 macrophages, and vascular endothelial cells. We demonstrate that 3D culture conditions enhance pathological phenotypes by upregulating FABP4 and activating the PI3K/AKT signaling pathway. This model accurately reflects the *in vivo* conditions of synovial tissue, exhibiting critical pathological behaviors such as inflammation, cell proliferation, migration, invasion, and angiogenesis. This versatile and physiologically relevant synovial organoid model not only provides a new platform for evaluating the efficacy of antirheumatic drugs, but also paves the way for in-depth study of the pathogenesis of RA. When integrated with advanced techniques such as single-cell imaging, sequencing, or gene editing, this model holds great promise for developing translational organoid models that provide insights into cellular interactions and their implications for treatment outcomes. Looking forward, the application of our synovial organoid model extends beyond RA, offering a versatile tool for exploring the mechanisms of various pathologies and testing bioactive compounds. Its ability to mimic complex cell-to-cell interactions in a controlled environment makes it an invaluable resource for advancing our understanding of disease processes and enhancing the development of targeted therapies.

CRediT authorship contribution statement

Xiaocheng Wang: Writing – original draft, Validation, Methodology, Investigation, Formal analysis, Data curation. **Jiaxin He:** Writing – review & editing, Validation, Methodology, Investigation, Formal analysis, Data curation. **Qiang Zhang:** Investigation, Data curation. **Juan He:** Validation, Data curation. **Qingwen Wang:** Writing – review & editing, Supervision, Resources, Project administration, Funding acquisition.

Declaration of competing interest

We would like to submit the enclosed manuscript entitled "Constructing a 3D co-culture *in vitro* synovial tissue model for rheumatoid arthritis research", which we wish to be considered for publication in ***Materials Today Bio***. The authors declare that they have no conflict of interest.

Acknowledgments

This study was supported by the National Natural Science Foundation of China (No. 81974253), Sanming Project of Medicine in Shenzhen (No. SZSM202311030), Treatment and Prevention Integration Project of Shenzhen Municipal Health Commission (No. 0102018-2019-YBXM-1499-01-0414), Shenzhen Key Laboratory of Inflammatory and Immunology Diseases (ZDSYS20200811143756018), Shenzhen Science and Technology Program (JCYJ20210324110011031 and RCBS20210706092212003), Shenzhen Medical Research Fund (C2301008), Key Project of Basic Research of Shenzhen Science and Technology Innovation Commission) (JCYJ20200109140203849) and Guangdong Basic and Applied Basic Research Foundation (No. 2023A1515010294).

Appendix A. Supplementary data

Supplementary data to this article can be found online at https://doi.org/10.1016/j.mtbio.2025.101492.

Data availability

Data will be made available on request.

References

[1] E.M. Gravallese, G.S. Firestein, Rheumatoid arthritis - common origins, Divergent mechanisms, N. Engl. J. Med. 388 (6) (2023) 529–542.
[2] M.H. Smith, J.R. Berman, What is rheumatoid arthritis? JAMA 327 (12) (2022) 1194.
[3] D. van der Heijde, V. Strand, Y. Tanaka, E. Keystone, J. Kremer, C.A.F. Zerbini, M. H. Cardiel, S. Cohen, P. Nash, Y.W. Song, D. Tegzová, D. Gruben, G. Wallenstein, C. A. Connell, R. Fleischmann, Tofacitinib in combination with methotrexate in patients with rheumatoid arthritis: clinical efficacy, radiographic, and safety outcomes from a twenty-four-month, phase III study, Arthritis Rheumatol. 71 (6) (2019) 878–891.
[4] Q. Ding, W. Hu, R. Wang, Q. Yang, M. Zhu, M. Li, J. Cai, P. Rose, J. Mao, Y.Z. Zhu, Signaling pathways in rheumatoid arthritis: implications for targeted therapy, Signal Transduct. Targeted Ther. 8 (1) (2023) 68.
[5] E. Ha, S.C. Bae, K. Kim, Large-scale meta-analysis across East Asian and European populations updated genetic architecture and variant-driven biology of rheumatoid arthritis, identifying 11 novel susceptibility loci, Ann. Rheum. Dis. 80 (5) (2021) 558–565.
[6] Z.A. Li, S. Sant, S.K. Cho, S.B. Goodman, B.A. Bunnell, R.S. Tuan, M.S. Gold, H. Lin, Synovial joint-on-a-chip for modeling arthritis: progress, pitfalls, and potential, Trends Biotechnol. 41 (4) (2023) 511–527.
[7] H. Kim, J.H. Back, G. Han, S.J. Lee, Y.E. Park, M.B. Gu, Y. Yang, J.E. Lee, S.H. Kim, Extracellular vesicle-guided in situ reprogramming of synovial macrophages for the treatment of rheumatoid arthritis, Biomaterials 286 (2022) 121578.
[8] M.G.A. Broeren, C.E.J. Waterborg, R. Wiegertjes, R.M. Thurlings, M.I. Koenders, P. Van Lent, P.M. Van der Kraan, F.A.J. Van de Loo, A three-dimensional model to study human synovial pathology, ALTEX 36 (1) (2019) 18–28.

[9] S. Kim, S. Min, Y.S. Choi, S.H. Jo, J.H. Jung, K. Han, J. Kim, S. An, Y.W. Ji, Y. G. Kim, S.W. Cho, Tissue extracellular matrix hydrogels as alternatives to Matrigel for culturing gastrointestinal organoids, Nat. Commun. 13 (1) (2022) 1692.
[10] M.T. Kozlowski, H.N. Zook, D.N. Chigumba, C.P. Johnstone, L.F. Caldera, H. P. Shih, D.A. Tirrell, H.T. Ku, A matrigel-free method for culture of pancreatic endocrine-like cells in defined protein-based hydrogels, Front. Bioeng. Biotechnol. 11 (2023) 1144209.
[11] D. Grimm, US EPA to eliminate all mammal testing by 2035, Science 365 (2019) 1231.
[12] C. Xie, R. Liang, J. Ye, Z. Peng, H. Sun, Q. Zhu, X. Shen, Y. Hong, H. Wu, W. Sun, X. Yao, J. Li, S. Zhang, X. Zhang, H. Ouyang, High-efficient engineering of osteo-callus organoids for rapid bone regeneration within one month, Biomaterials 288 (2022) 121741.
[13] X. Luo, E.L.S. Fong, C. Zhu, Q.X.X. Lin, M. Xiong, A. Li, T. Li, T. Benoukraf, H. Yu, S. Liu, Hydrogel-based colorectal cancer organoid co-culture models, Acta Biomater. 132 (2021) 461–472.
[14] N. O'Donnell, I.A. Okkelman, P. Timashev, T.I. Gromovykh, D.B. Papkovsky, R. I. Dmitriev, Cellulose-based scaffolds for fluorescence lifetime imaging-assisted tissue engineering, Acta Biomater. 80 (2018) 85–96.
[15] I.A.A. Fernandes, A.C. Pedro, V.R. Ribeiro, D.G. Bortolini, M.S.C. Ozaki, G. M. Maciel, C.W.I. Haminiuk, Bacterial cellulose: from production optimization to new applications, Int. J. Biol. Macromol. 164 (2020) 2598–2611.
[16] C. Chen, W. Ding, H. Zhang, L. Zhang, Y. Huang, M. Fan, J. Yang, D. Sun, Bacterial cellulose-based biomaterials: from fabrication to application, Carbohydr. Polym. 278 (2022) 118995.
[17] L. Liu, X. Ji, L. Mao, L. Wang, K. Chen, Z. Shi, A.A.Q. Ahmed, S. Thomas, R. V. Vasilievich, L. Xiao, X. Li, G. Yang, Hierarchical-structured bacterial cellulose/potato starch tubes as potential small-diameter vascular grafts, Carbohydr. Polym. 281 (2022) 119034.
[18] X. Liu, M. Wu, M. Wang, Q. Hu, J. Liu, Y. Duan, B. Liu, Direct synthesis of photosensitizable bacterial cellulose as engineered living material for skin wound repair, Adv. Mater. 34 (13) (2022) e2109010.
[19] H. Chen, X. Wang, J. Wang, X. Shi, X. Li, J. Wang, D. Li, Y. Zhu, W. Tan, Z. Tan, In vitroadipogenesis and long-term adipocyte culture in adipose tissue-derived cell banks, Biofabrication 13 (3) (2021).
[20] D. Guo, C. Lin, Y. Lu, H. Guan, W. Qi, H. Zhang, Y. Shao, C. Zeng, R. Zhang, H. Zhang, X. Bai, D. Cai, FABP4 secreted by M1-polarized macrophages promotes synovitis and angiogenesis to exacerbate rheumatoid arthritis, Bone Res 10 (1) (2022) 45.
[21] G.S. Hotamisligil, D.A. Bernlohr, Metabolic functions of FABPs–mechanisms and therapeutic implications, Nat. Rev. Endocrinol. 11 (10) (2015) 592–605.
[22] X.N. Ge, I. Bastan, M. Dileepan, Y. Greenberg, S.G. Ha, K.A. Steen, D.A. Bernlohr, S. P. Rao, P. Sriramarao, FABP4 regulates eosinophil recruitment and activation in allergic airway inflammation, Am. J. Physiol. Lung Cell Mol. Physiol. 315 (2) (2018) L227–l240.
[23] S. Chen, J. Du, W. Zhao, R. Cao, N. Wang, J. Li, B. Shen, S. Chen, Elevated expression of FABP4 is associated with disease activity in rheumatoid arthritis patients, Biomarkers Med. 14 (15) (2020) 1405–1413.
[24] I.A. Udalova, A. Mantovani, M. Feldmann, Macrophage heterogeneity in the context of rheumatoid arthritis, Nat. Rev. Rheumatol. 12 (8) (2016) 472–485.
[25] H.Y. Yap, S.Z. Tee, M.M. Wong, S.K. Chow, S.C. Peh, S.Y. Teow, Pathogenic role of immune cells in rheumatoid arthritis: implications in clinical treatment and biomarker development, Cells 7 (10) (2018).
[26] Y. Kaneko, T. Takeuchi, Targeted antibody therapy and relevant novel biomarkers for precision medicine for rheumatoid arthritis, Int. Immunol. 29 (11) (2017) 511–517.
[27] M. Narazaki, T. Tanaka, T. Kishimoto, The role and therapeutic targeting of IL-6 in rheumatoid arthritis, Expet Rev. Clin. Immunol. 13 (6) (2017) 535–551.
[28] M. Akiyama, Y. Kaneko, Pathogenesis, clinical features, and treatment strategy for rheumatoid arthritis-associated interstitial lung disease, Autoimmun. Rev. 21 (5) (2022) 103056.
[29] X.C. Wang, R.B. Zhao, J. Wang, X.H. Li, L.J. Jin, W.Y. Liu, L.F. Yang, Y.H. Zhu, Z. K. Tan, 3D-printed tissue repair patch combining mechanical support and magnetism for controlled skeletal muscle regeneration, Bio-Design and Manufacturing 5 (2) (2022) 249–264.
[30] M.A. Naeem, M. Alfred, P. Lv, H. Zhou, Q. Wei, Three-dimensional bacterial cellulose-electrospun membrane hybrid structures fabricated through in-situ self-assembly, Cellulose 25 (12) (2018) 6823–6830.
[31] K. Chen, Z.W. Lin, S.M. He, C.Q. Wang, J.C. Yang, Y. Lu, X.B. Xie, Q. Li, Metformin inhibits the proliferation of rheumatoid arthritis fibroblast-like synoviocytes through IGF-IR/PI3K/AKT/m-TOR pathway, Biomed. Pharmacother. 115 (2019) 108875.
[32] G. Nygaard, G.S. Firestein, Restoring synovial homeostasis in rheumatoid arthritis by targeting fibroblast-like synoviocytes, Nat. Rev. Rheumatol. 16 (6) (2020) 316–333.
[33] H. Chen, Y. Cheng, X. Wang, J. Wang, X. Shi, X. Li, W. Tan, Z. Tan, 3D printed in vitro tumor tissue model of colorectal cancer, Theranostics 10 (26) (2020) 12127–12143.
[34] O. Boucherat, V. Agrawal, A. Lawrie, S. Bonnet, The latest in animal models of pulmonary hypertension and right ventricular failure, Circ. Res. 130 (9) (2022) 1466–1486.
[35] X. Wang, L. Jin, W. Liu, L. Stingelin, P. Zhang, Z. Tan, Construction of engineered 3D islet micro-tissue using porcine decellularized ECM for the treatment of diabetes, Biomater. Sci. 11 (16) (2023) 5517–5532.
[36] S.A. Yi, Y. Zhang, C. Rathnam, T. Pongkulapa, K.B. Lee, Bioengineering approaches for the advanced organoid research, Adv. Mater. 33 (45) (2021) e2007949.
[37] M. Rothbauer, R.A. Byrne, S. Schobesberger, I. Olmos Calvo, A. Fischer, E.I. Reihs, S. Spitz, B. Bachmann, F. Sevelda, J. Holinka, W. Holnthoner, H. Redl, S. Toegel, R. Windhager, H.P. Kiener, P. Ertl, Establishment of a human three-dimensional chip-based chondro-synovial coculture joint model for reciprocal cross talk studies in arthritis research, Lab Chip 21 (21) (2021) 4128–4143.
[38] M. Zhu, W. Li, X. Dong, X. Yuan, A.C. Midgley, H. Chang, Y. Wang, H. Wang, K. Wang, P.X. Ma, H. Wang, D. Kong, In vivo engineered extracellular matrix scaffolds with instructive niches for oriented tissue regeneration, Nat. Commun. 10 (1) (2019) 4620.
[39] C.D. Buckley, C. Ospelt, S. Gay, K.S. Midwood, Location, location, location: how the tissue microenvironment affects inflammation in RA, Nat. Rev. Rheumatol. 17 (4) (2021) 195–212.
[40] E.M.L. Philippon, L.J.E. van Rooijen, F. Khodadust, J.P. van Hamburg, C.J. van der Laken, S.W. Tas, A novel 3D spheroid model of rheumatoid arthritis synovial tissue incorporating fibroblasts, endothelial cells, and macrophages, Front. Immunol. 14 (2023) 1188835.
[41] L. Neufeld, E. Yeini, N. Reisman, Y. Shtilerman, D. Ben-Shushan, S. Pozzi, A. Madi, G. Tiram, A. Eldar-Boock, S. Ferber, R. Grossman, Z. Ram, R. Satchi-Fainaro, Microengineered perfusable 3D-bioprinted glioblastoma model for in vivo mimicry of tumor microenvironment, Sci. Adv. 7 (34) (2021).
[42] X.Y. Tang, S. Wu, D. Wang, C. Chu, Y. Hong, M. Tao, H. Hu, M. Xu, X. Guo, Y. Liu, Human organoids in basic research and clinical applications, Signal Transduct. Targeted Ther. 7 (1) (2022) 168.
[43] Y. Sun, W. Liu, H. Zhang, H. Li, J. Liu, F. Zhang, T. Jiang, S. Jiang, Curcumin prevents osteoarthritis by inhibiting the activation of inflammasome NLRP3, J. Interferon Cytokine Res. 37 (10) (2017) 449–455.
[44] Y.P. Singh, J.C. Moses, N. Bhardwaj, B.B. Mandal, Overcoming the dependence on animal models for osteoarthritis therapeutics - the promises and prospects of in vitro models, Adv. Healthcare Mater. 10 (20) (2021) e2100961.
[45] A.M. Boniakowski, A.D. denDekker, F.M. Davis, A. Joshi, A.S. Kimball, M. Schaller, R. Allen, J. Bermick, D. Nycz, M.E. Skinner, S. Robinson, A.T. Obi, B.B. Moore, J. E. Gudjonsson, D. Lombard, S.L. Kunkel, K.A. Gallagher, SIRT3 regulates macrophage-mediated inflammation in diabetic wound repair, J. Invest. Dermatol. 139 (12) (2019) 2528–2537.e2.
[46] J. Zhang, Y. Xu, C. Zhuo, R. Shi, H. Wang, Z. Hu, H.F. Chan, H.W. Kim, Y. Tao, M. Li, Highly efficient fabrication of functional hepatocyte spheroids by a magnetic system for the rescue of acute liver failure, Biomaterials 294 (2023) 122014.
[47] V. Brancato, F. Gioiella, M. Profeta, G. Imparato, D. Guarnieri, F. Urciuolo, P. Melone, P.A. Netti, 3D tumor microtissues as an in vitro testing platform for microenvironmentally-triggered drug delivery systems, Acta Biomater. 57 (2017) 47–58.
[48] M. Kurowska-Stolarska, S. Alivernini, Synovial tissue macrophages in joint homeostasis, rheumatoid arthritis and disease remission, Nat. Rev. Rheumatol. 18 (7) (2022) 384–397.